MTL TR 89-70

AD

BIAXIAL FLEXING OF A FIBER-REINFORCED ALUMINUM COMPOSITE

NIKOS TSANGARAKIS and MARC S. PEPI
MATERIALS TESTING AND EVALUATION BRANCH

July 1989

US ARMY
LABORATORY COMMAND
MATERIALS TECHNOLOGY LABORATORY

U.S. ARMY MATERIALS TECHNOLOGY LABORATORY
Watertown, Massachusetts 02172-0001

The findings in this report are not to be construed as an official Department of the Army position, unless so designated by other authorized documents.

Mention of any trade names or manufacturers in this report shall not be construed as advertising nor as an official indorsement or approval of such products or companies by the United States Government.

DISPOSITION INSTRUCTIONS

Destroy this report when it is no longer needed.
Do not return it to the originator.

UNCLASSIFIED

SECURITY CLASSIFICATION OF THIS PAGE *(When Data Entered)*

REPORT DOCUMENTATION PAGE		READ INSTRUCTIONS BEFORE COMPLETING FORM
1. REPORT NUMBER MTL TR 89-70	2. GOVT ACCESSION NO.	3. RECIPIENT'S CATALOG NUMBER
4. TITLE *(and Subtitle)* BIAXIAL FLEXING OF A FIBER-REINFORCED ALUMINUM COMPOSITE		5. TYPE OF REPORT & PERIOD COVERED Final Report 6. PERFORMING ORG. REPORT NUMBER
7. AUTHOR(s) Nikos Tsangarakis and Marc S. Pepi		8. CONTRACT OR GRANT NUMBER(s)
9. PERFORMING ORGANIZATION NAME AND ADDRESS U.S. Army Materials Technology Laboratory Watertown, Massachusetts 02172-0001 SLCMT-MRD		10. PROGRAM ELEMENT, PROJECT, TASK AREA & WORK UNIT NUMBERS D/A Project: 1L162105.AH42
11. CONTROLLING OFFICE NAME AND ADDRESS U.S. Army Laboratory Command 2800 Powder Mill Road Adelphi, Maryland 20783-1145		12. REPORT DATE July 1989 13. NUMBER OF PAGES 17
14. MONITORING AGENCY NAME & ADDRESS *(if different from Controlling Office)*		15. SECURITY CLASS. *(of this report)* Unclassified 15a. DECLASSIFICATION/DOWNGRADING SCHEDULE

16. DISTRIBUTION STATEMENT *(of this Report)*

Approved for public release; distribution unlimited.

17. DISTRIBUTION STATEMENT *(of the abstract entered in Block 20, if different from Report)*

18. SUPPLEMENTARY NOTES

19. KEY WORDS *(Continue on reverse side if necessary and identify by block number)*

Fiber composites
Metal-matrix composites
Biaxial loading
Biaxial fatigue

20. ABSTRACT *(Continue on reverse side if necessary and identify by block number)*

(SEE REVERSE SIDE)

DD FORM 1 JAN 73 1473 EDITION OF 1 NOV 65 IS OBSOLETE

UNCLASSIFIED

SECURITY CLASSIFICATION OF THIS PAGE *(When Data Entered)*

Block No. 20

ABSTRACT

Disks of silicon carbide continuous fiber-reinforced $[(0^6/90^6)_{4S}]$ aluminum were supported circumferentially on one side and loaded at the center of the other side with a pin. Maxima principal tensile surface strains were determined during flexing with strain gages.

Failure under monotonic loading initiated on the convex side of the disks with the formation of multiple breaks in the first layer of fibers. With further flexing, cracking extended to inner fiber layers. Finally, fracture extended through the convex surface layer of the aluminum matrix. On cyclic flexing, fiber cracking was found to be the failure mechanism whenever the cyclic principal surface strain range was 0.0035 or greater. For cyclic strain ranges less than 0.0035, slip bands and cracks were formed in the matrix in addition to the cracks formed in the fibers. The cyclic strain range limit for $\sim 10^6$ cycles of life was found to approach 0.0015. The latter limit corresponded to a maximum cyclic fiber strain of 0.00132, which is only 15% of the fiber strain to failure under monotonic uniaxial composite loading.

CONTENTS

INTRODUCTION

The introduction of fiber-reinforced composites in structural design has created the need to develop new test procedures for rating these materials. The assessment of the performance of such composites under biaxial loading should increase their reliability and applicability. Specimens such as the cruciform,[1-4] the thin wall cylinder,[5-11] and the center-cracked plate[12] have been used extensively to investigate the response of isotropic materials to biaxial loading. These three specimens, however, may not be appropriate for all types of fiber-reinforced composites. It has been shown that in certain composites, premature failure by fiber debonding can initiate at locations of stress concentration or where a change in the specimen's contours exists.[13,14] Because of these trends, the cruciform and the center-cracked plate could be poor candidates for biaxial testing of fiber-reinforced composites, especially those reinforced unidirectionally. The thin wall cylindrical specimen, on the other hand, could be promising for certain applications (i.e., pressure vessels) provided that the cost of producing it or its availability are not problematic.[15]

Several investigators have used a circumferentially clamped disk, pressurized from one side, to conduct biaxial testing of metallic materials.[16-20] Shetty et al.,[21] developed a fixture for testing ceramic disks in biaxial flexure. Shetty used pressurized mercury to uniformly load Al_2O_3 disks on one side, while the other side was freely supported circumferentially. Quinn and Wirth[22] loaded Si_3N_4 disks with a small hollow cylinder.

In the present study, an approach similar to Quinn's is used to assess the response of a silicon carbon continuous fiber-reinforced aluminum composite to biaxial tensile flexure. A test parameter which relates to failure initiation is identified and used to characterize the performance of the composite.

MATERIALS, SPECIMENS, AND TEST PROCEDURES

Plates (25 cm x 25 cm) of 6061 aluminum (not containing significant amounts of Li) reinforced with continuous fibers (0.14-mm diameter) of silicon carbide (SiC_f/Al) were procured from AVCO. The cross-ply $[(0^\circ/90^\circ)_{4S}]$ composite plates were 1.6-mm thick. The fiber volume content of the composites was 45% to 47%. The $(0^\circ/90^\circ)_{4S}$ [and (0°) for comparison] composite properties[14] are listed in Table 1. The fiber modulus of elasticity, the ultimate tensile strength, and the Poisson's ratio were 386 GPa, 2992 MPa to 3289 MPa, and 0.19, respectively.[23] Typical values of the ultimate tensile strength, the 0.2% offset yield strength, and the endurance limit of the 6061 aluminum matrix (T6 condition) are 290 MPa, 262 MPa, and 193 MPa, respectively.[24] The matrix modulus of elasticity can be assumed to be 69 GPa.

Disks with a diameter of 50.8 mm were cut with a cylindrical hollow diamond drill using an appropriate fluid as coolant and lubricant and at 3500 rpm cutting speed. These disks were used to conduct biaxial tension-tension flexural tests.

Table 1. TYPICAL COMPOSITE MECHANICAL PROPERTIES

Material	Test Direction	UTS(MPa)*	E(GPa)†	V‡	e_f**
SiC_f/Al (0°)	Parallel to Fibers	1273	204	0.27	0.0089
SiC_f/Al (0°)	Normal to Fibers	76	118	0.125	0.0008
SiC_f/Al - $(0°/90°)_{4S}$	Along the 0° Fibers	629	136	–	0.0090

*UTS = ultimate tensile strength
†E = Young's modulus
‡V = Poisson's ratio
**e_f = fracture strain

To conduct a biaxial flexure test, the composite disk was positioned on a steel supporting ring, whose outside and inside diameters were 50.8 mm and 48.8 mm, respectively. Load was transferred to the disk with a 12.2-mm diameter, 25-mm-long steel cylinder (Figure 1). Static tests were conducted at a displacement rate of 1 mm/min. Flexural cyclic tests were conducted at frequencies of 0.01, 1, and 4 Hz for fatigue lives of 0-500, 500-10^4, 10^4, and more cycles, respectively. In all fatigue tests, the first two cycles were conducted under manual control. A recoverable strain range (Figure 2) was determined as the difference between the total strain at peak load and the residual (after load removal) strain. This strain range will be discussed in greater detail in a subsequent section. Because the minimum strain (point C in Figure 2) in these cyclic tests was practically zero, the R value (ratio of the minium strain divided by the maximum strain) was zero. The load-strain relationship was monitored with a digital oscilloscope and the load was varied appropriately so as to keep the strain range constant during cyclic flexure. Plots of load versus strain were made periodically under manual machine control with a X-Y recorder. The slope of segment BC in Figure 2 will be referred to hereafter as the stiffness.

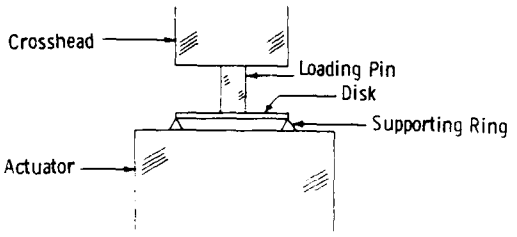

Figure 1. Loading arrangement for biaxial flexure.

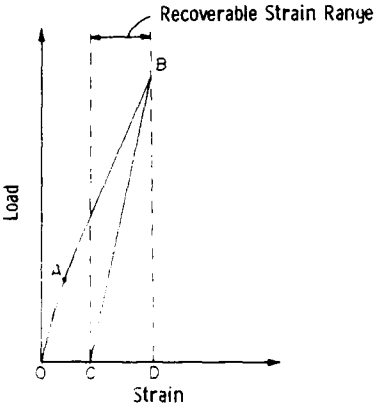

Figure 2. Definition of recoverable strain range.

The displacements of the loading pin and the disk's center were monitored with the Instron's actuator displacement transducer and a LVDT, respectively. The two displacements were found to be nearly identical (any difference was less than 0.05 mm). Strain measurements were determined with 1 mm x 1 mm, 350 ohm resistance strain gages which were positioned on the disks at a strategic location. This position was determined experimentally.

Metallographic examination of specimens was conducted to determine the nature and the extent of the damage generated during testing. Because of a residual curvature in many tested disks, detection of this damage by ultrasonic C-scans[25] was abandoned. X-ray examinations failed to detect the generated damage.

EXPERIMENTAL RESULTS

The Response Monitoring Parameter and Strain Distributions

The displacement of the center of the disks during flexural loading was first examined as a material response monitoring parameter. The relationship between this displacement and the applied load is depicted in Figure 3. The reproducibility of the curve presented a variability of ± 8%. It was found, however, that the relationship between displacement and load was not sensitive to localized composite yielding (which initiated at 410 N) and to damage generated in the composite during the flexural loading.

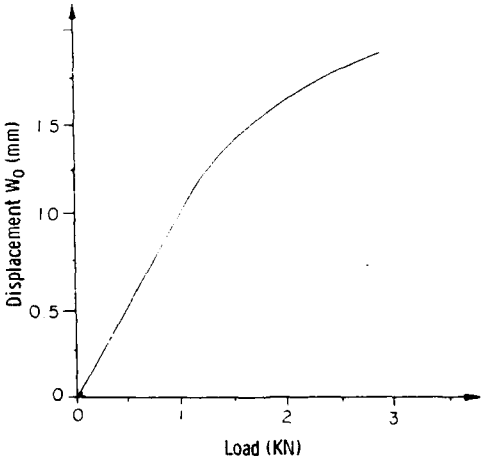

Figure 3. Relationship of loads and displacements.

The principal strain e_{zz}, which was through the thickness of the disks, was compressive and maximum at the centers of their concave (during flexure) sides and vanished on their convex sides. However, for the load range used in these tests, the maximum absolute value of this principal strain was at least one order of magnitude less than the maximum value of the other two principal strains. Thus, under flexural loading, the concave surface of the disk was under triaxial compression (within the loading pin area) and the convex surface was under biaxial tension.

The strain distribution on the convex surface of the disks was mapped during flexing to determine the maxima in the tensile strains which would then be used to assess the composite response. The distribution of these surface tensile strains was determined from measurements with strain gages. The surface tensile strains along the principal directions X and Y (X and Y parallel to the 0° and 90° fibers, respectively) were found to be constant and equal to each other within a radius of 6.1 mm from the centers of the disks (within the boundary ADBC in Figure 4). The principal surface strains decreased with distance from this boundary

to zero at the edges of the disks (points E, G, F, H). Because of the magnitude of these strains, and knowing that ceramics are sensitive to tension rather than compression, it was felt that failure of the composite would initiate within the boundary ADBC. The disks symmetry planes were found (from measurements with strain gages) to be coincident with their neutral planes during flexure. Thus, assuming good bonding between the matrix and the fibers, a linear relationship existed between the magnitude of the principal strain and its distance from the neutral plane. The principal fiber strain e_{xx}, however, being the furthest from the neutral plane was also the greatest. Thus, the surface principal strain e_{xx} was chosen as the material response monitoring parameter and was retrieved during flexure with a strain gage which was positioned at 5 mm from the center of the disks.

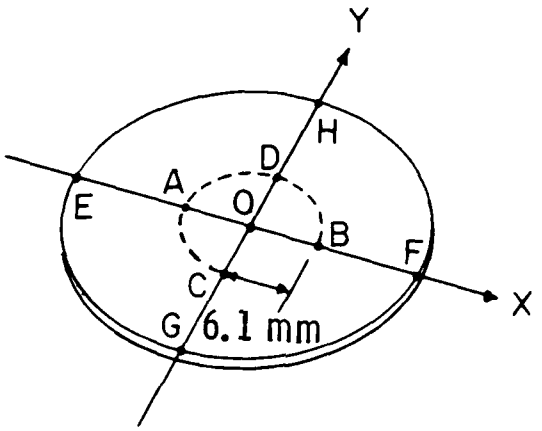

Cross-Ply Composite

Figure 4. Strain distributions.

Monotonic Flexural Response

The response (surface principal strain e_{xx}) of a typical composite disk to the flexural biaxial tensile loading is depicted in Figure 5. The initial stiffness on loading was 259 KN/cm/cm. After point A (410 N), a change in the slope of the curve is evident. This change in slope was associated with matrix yielding which introduced a minute curvature in disks which were tested beyond point A. Because of this curvature, damage detection by C-scans became a very cumbersome procedure and, thus, was abandoned. The value of the stiffness at point B was 482 KN/cm/cm. In the author's opinion, this increase in stiffness was the result of a combination of strain hardening of the aluminum matrix and the removal of internal residual stresses by plastic deformation of the aluminum matrix. Johnson[26] used the same justification for an increasing stiffness during the cyclic tension-tension uniaxial loading of B/Al coupons. The internal residual stresses were introduced in the composite on cooling to room temperature after thermal processing. During cooling, the matrix was forced into tension by the ceramic fibers because of a difference in thermal contraction. Thus, in the as-received condition, the aluminum matrix suffers an elastic, thermally induced tensile strain.[27] A permanent strain of 0.00177 was noticed after removing the load (point C). On reloading the specimen,

a hysterisis loop was formed and the load-strain curve returned to point B (1268 N load). At point D, the load was 2450 N and the total strain was 0.0095. With further increase in load, a decrease in the slope of the curve incurred and the load reached a maximum of 2900 N (point E). At point E (strain e_{xx} of 0.01225), the load was removed. The residual strain was 0.0044 (point F). The stiffness at point E was 369 KN/cm/cm. This stiffness (ignoring the boomerang shape of the segment EF which was attributed to a surface crack) was less than that at point B. This decrease in stiffness was caused by damage which was introduced in the composite during loading.

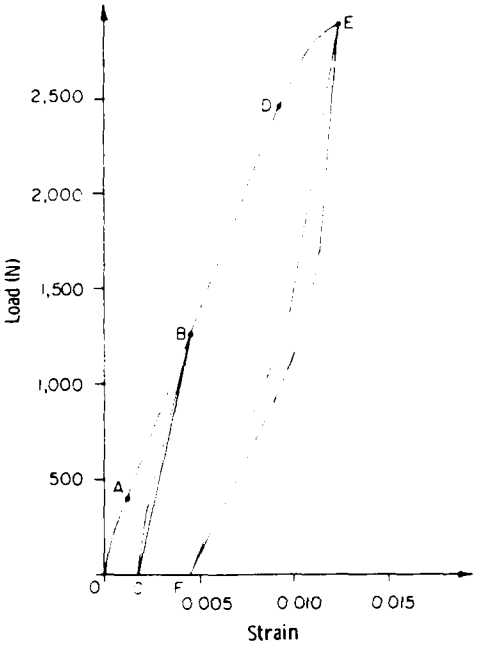

Figure 5. Response of the cross-ply composite to monotonic biaxial tension-tension flexure.

Cyclic Flexural Response

The cyclic flexural behavior of a typical disk is depicted in Figure 6. The disk was initially loaded to 1268 N and then unloaded. The total surface principal strain at peak load was 0.0056 and the residual strain (after unloading) was 0.00177. Thus, the recoverable surface principal strain range was 0.00383 and the initial stiffness was 331 KN/cm/cm. Cyclic flexing within this strain range continued and sequential plots of load versus strain were made to evaluate the stiffness degradation and the decrease in the maximum cyclic load applied to the disk as functions of the fatigue cycles. The decrease in the maximum cyclic load was necessary in order to maintain the surface principal strain range constant during testing. After 16 cycles, the peak load had decreased by 322 N. This decrement was 25.4% of the original peak load and was attributed to damage introduced in the composite during flexing. Fatigue cycling under constant strain range was continued to 38 cycles without any further decrease in the peak load. This was interpreted as an indication that a state of saturation in the extent of fatigue damage had been reached in the composite. The peak load at this point was 946 N and, assuming elastic behavior, it corresponded to a residual stiffness of 247 KN/cm/cm. The bending of the lower portion of the curve into a boomerang shape after the 16th cycle was attributed to a crack which extended through the surface matrix layer.

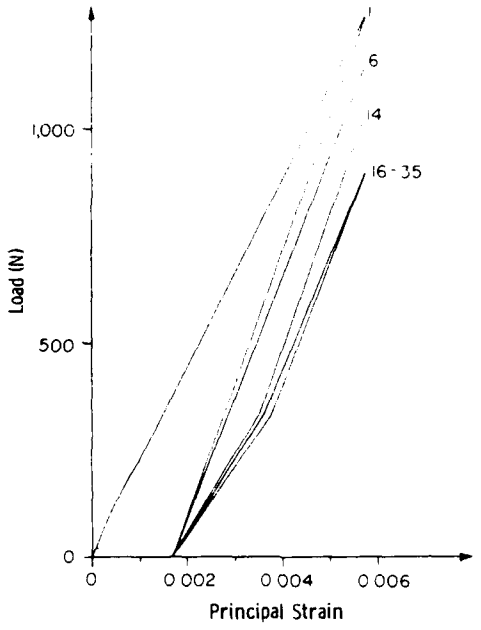

Figure 6. Response of a cross-ply disk (A10) to biaxial tension-tension cyclic flexure.

Fatigue data were generated for various surface principal strain ranges. The results of these tests are depicted in Figure 7. The points shown represent failures which corresponded to a 10% decrease in the load-carrying capacity of the disks. The dashed line represents the border below which no failures were observed. The limiting surface cyclic principal strain range for a fatigue life of 10^6 cycles is approaching the value of 0.0015, which corresponds to a maximum cyclic tensile fiber strain range of 0.00132. This latter strain is only 15% of the strain to failure of the composite under uniaxial monotonic loading (see Table 1).

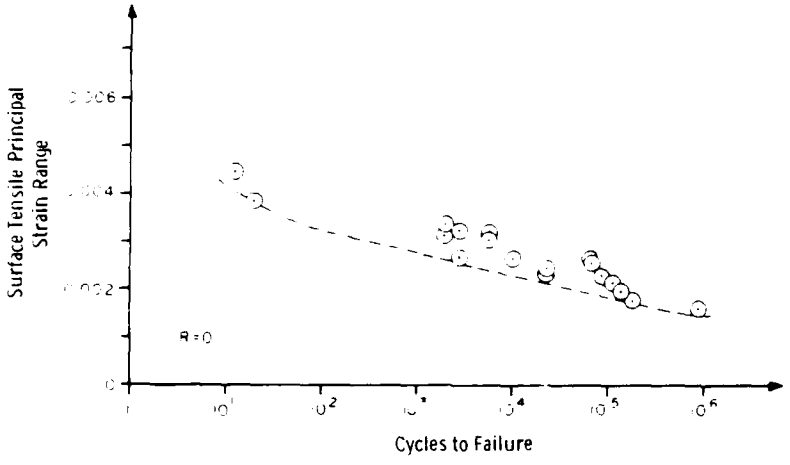

Figure 7. Biaxial tension-tension fatigue of $(0°/90°)_{4S}$ SiC/Al-45$^{v}/_{o}$ fiber.

Assessment of the Damage

Failure of the composite disks under monotonic loading initiated on the convex side (tension) with the formation of multiple cracks in the nearest to the surface layer of fibers. The formation of these fiber breaks initiated between points B and D of Figure 5. At these two points, the maxima tensile fiber strains were 0.0038 and 0.0083, respectively. With further flexing, cracking extended to the first layer of 90° fibers and then the second layer of the 0° fibers. Finally, fracture extended through the surface layer of the aluminum matrix (Figure 8). The cracks shown in Figure 8 had their planes parallel to the thickness of the disk and were within a 5-mm radius from the center of the disk. The boundaries of these cracks guided the authors in the strain gage site selection for the assessment of the composite response to the biaxial flexural tensile loading. With further loading, the cracks linked up to form an oval-shaped ring crack. A parallel to the 90° fibers, radial crack was also formed at this later stage (Figure 8). No fiber breaks were found in the compression side of the flexed disks.

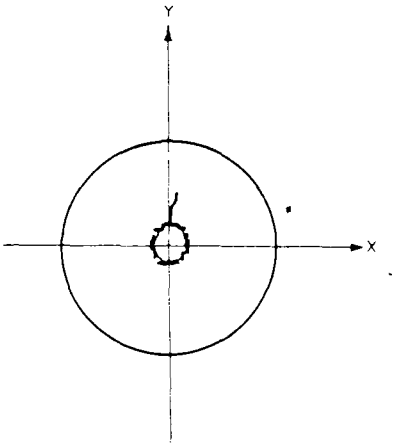

Figure 8. Surface cracks in a cross-ply composite disk.

The fiber breaks in the first 0° and 90° fiber layers shown in Figure 9 and Figure 10, respectively, were formed under a cyclic surface principal tensile strain range of 0.0039, and after 28 cycles of flexural loading. The average number of fiber breaks per unit length was 2 mm to 3 mm. These fiber breaks defined a damage zone which spread to a radius of 5 mm around the disk's center. The top portion of the second layer of 0° fibers was also cracked (Figure 9). The partially cracked fibers indicated that crack arrest action had occurred. The latter action implied that a minimum in the cyclic loading conditions for crack propagation had been reached. Assuming a linear relationship between strain and distance from the neutral plane (during flexure), the corresponding maximum cyclic fiber strain in this fiber layer was 0.0024. Fatigue-generated slip bands in the matrix were frequent. These slip bands (shown by arrow in Figure 11) were found to be always associated with the fiber/matrix interface and were indicative of a shearing action. This tendency of the matrix to shear during flexure led to the nucleation and development of the parallel to the plies crack shown in Figure 12. This crack was bridging the top of the first 0° layer of fibers. In several disks, a similar shearing action had initiated multiple cracks which were parallel to the plies, but not bridged to a single crack. These shear cracks were formed whenever the surface cyclic

principal strain range was less than 0.0035. This strain range value should be expected to be dependent on the degree of bonding of the matrix onto the fibers. In the author's opinion, the shear cracks were nucleated from the slip bands shown in Figure 11.

A disk which sustained a cyclic surface principal strain range of 0.003 for 6,000 cycles, exhibited fiber breaks which extended in the first layer of 90° fibers with a density of 0.5 mm. Shear cracks bridging the fibers were also detected in this disk. These cracks were more profound in the tension side of the disk (Figure 13). An additional feature of fatigue damage became evident during the metallographic examination of this disk. Matrix cracks which formed a 30° angle with the disk's thickness formed on both the tensile and compressive sides of the disk. These cracks are depicted in Figure 14 (indicated by the arrow). Numerous cracks through the aluminum matrix surface layer were also detected (Figures 13 and 14). The latter cracks were common in most tested disks and should not be associated with the cracks depicted in Figure 8. The cracks shown in Figure 8 were formed under monotonic loading.

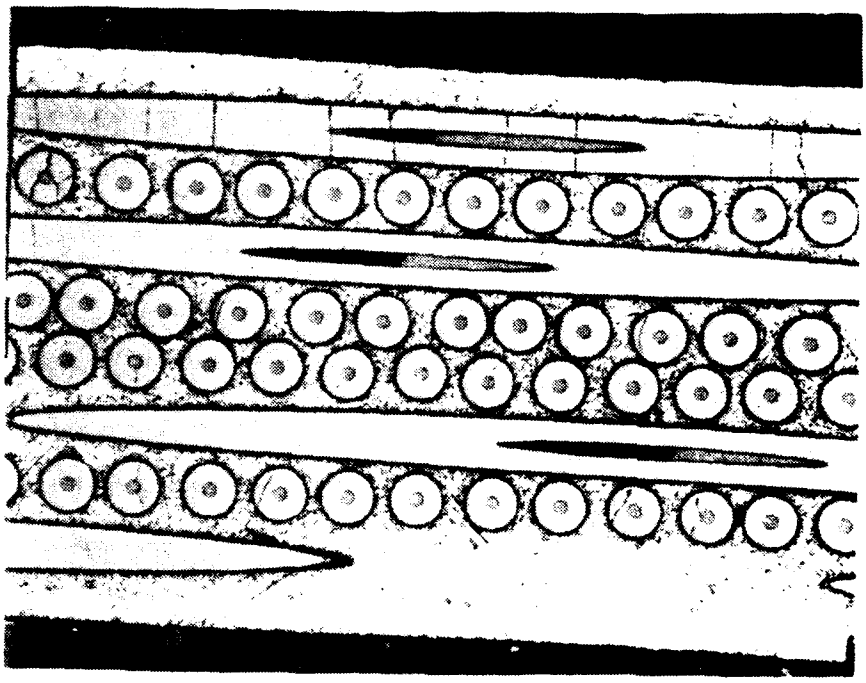

Figure 9. Damage of the 0° fibers in a cross-ply disk.

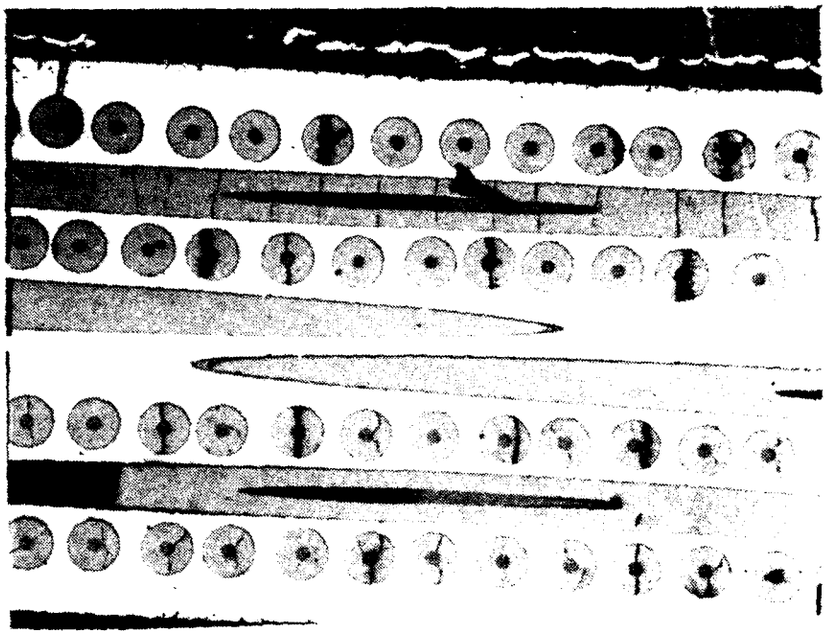

Figure 10. Damage of the 90° fibers in a cross-ply disk.

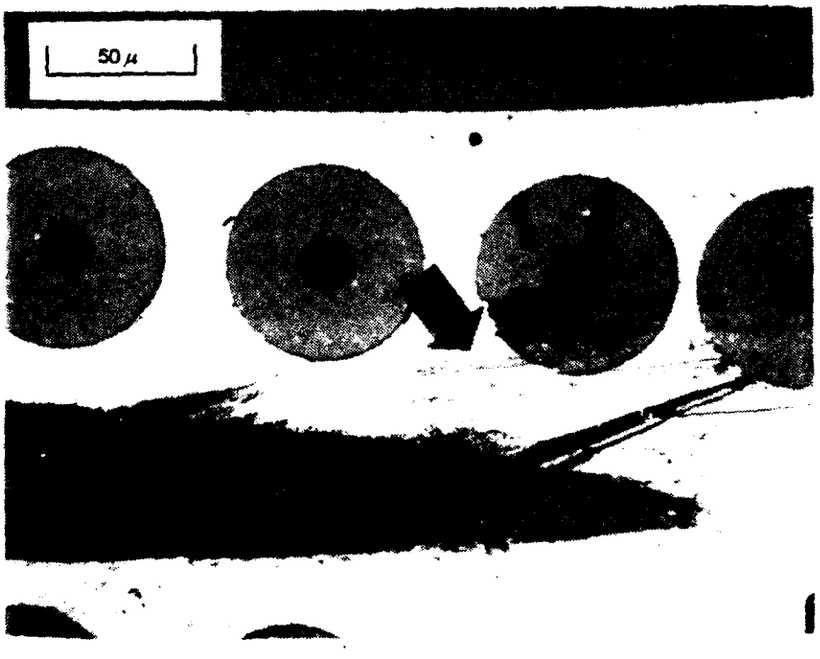

Figure 11. Slip bands in a cross-ply disk.

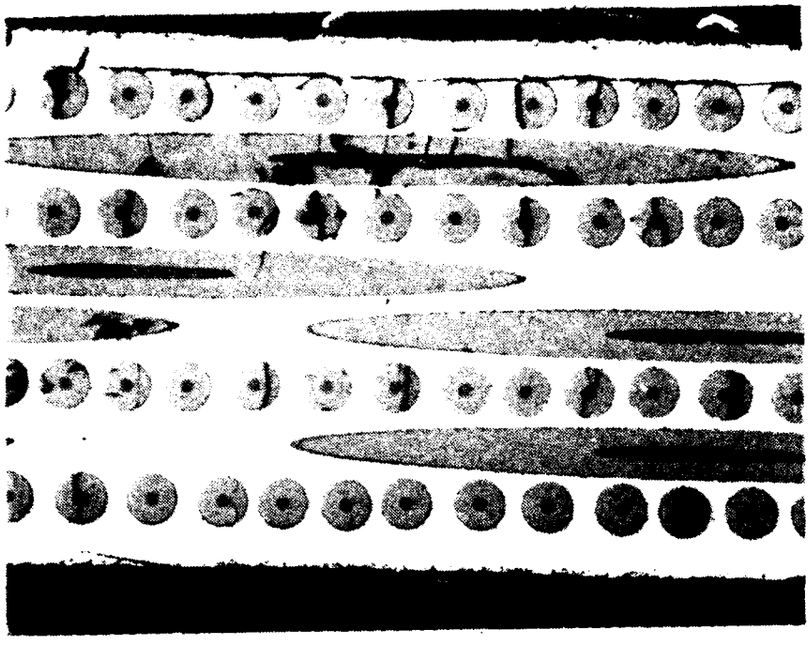

Figure 12. Parallel to the plies cracks in a cross-ply disk.

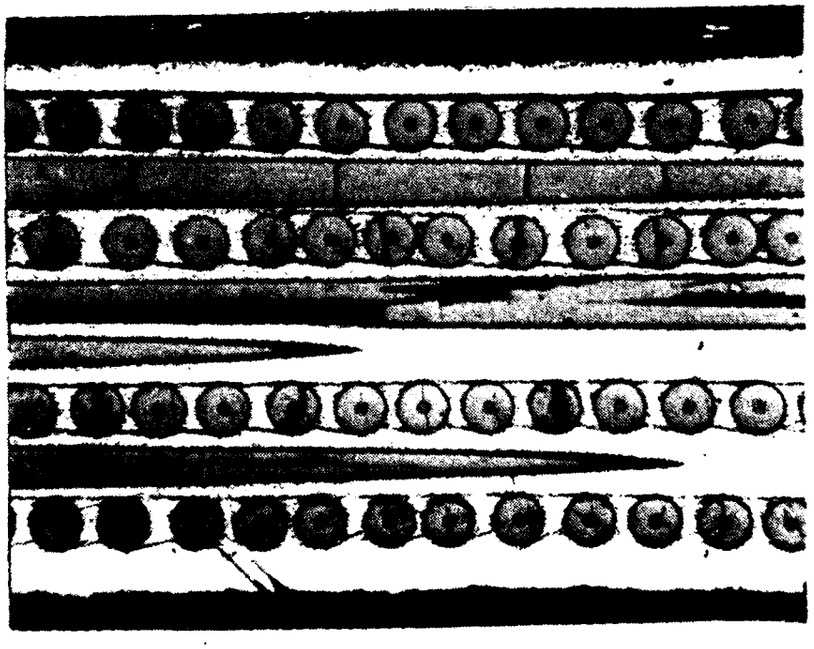

Figure 13. Multiple shear cracks in a cross-ply disk.

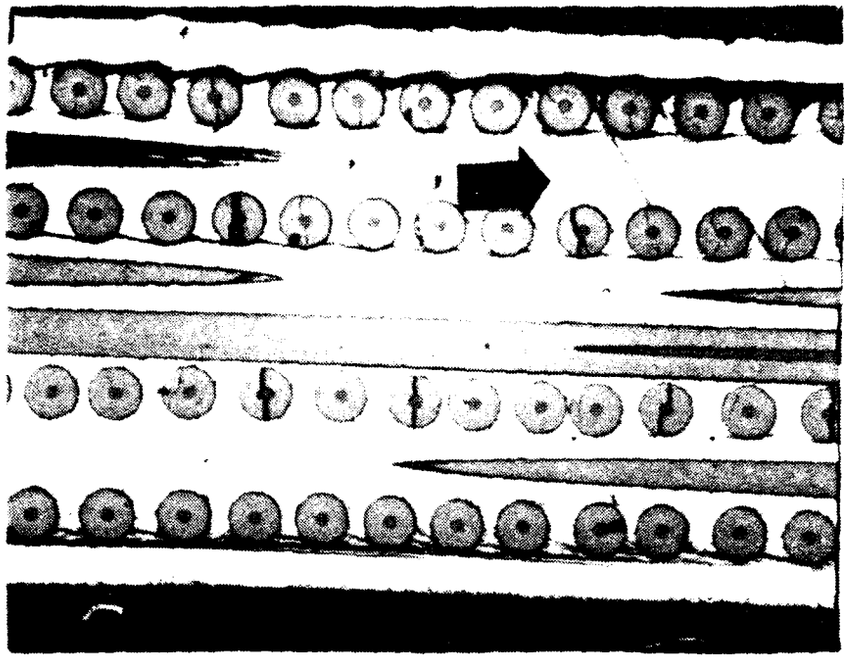

Figure 14. Inclined cracks in a cross-ply disk.

DISCUSSION

Although the relationship between the displacement of the center of the disk and the applied load could provide useful information about the damage introduced in the composite, it reflected a material response of the entire specimen. Thus, it represented a gross composite response and, as such, it was not as sensitive to localized damage as was the maximum principal tensile strain. The strain gage signal was associated with a maximum tensile loading only and, thus, it was directly related to the damage introduced in the tension side of the disk during flexing.

The selection of the parallel to the 0° fibers principal surface strain as the composite response monitoring parameter was based on the fact that these fibers suffered the maximum tensile strain during flexure. This was because these fibers were the farthest from the neutral plane of the flexed disk; thus, they were expected to fail first. The positioning of the strain gages monitoring this principal strain at 5 mm from the disks' centers was based on experimental observations on the location of the final through the matrix cracks. These cracks, shown in Figure 8, initiated within the segment DE of Figure 5. As was discussed earlier, the primary cracks were always forming within a distance of 5 mm around the disks' centers. This finding was significant because it indicated that the final failure initiated within a uniform principal surface strain field. The latter was found to extend 6.1 mm from the disks' centers. This boundary was found to also be the envelope of the composite damage which was generated during the cyclic flexing.

Metallographic examination of a number of tested disks indicated that cracking of the first 0° fiber layer initiated between points B and D of Figure 5. At points B and D, the

surface principal strains were 0.0043 and 0.0095, respectively. The related maxima tensile fiber strains were 0.0038 and 0.0083. Fracture extended to inner fiber layers as loading approached point E. Near point E, the four primary surface cracks of Figure 8 were formed. These cracks were responsible for the boomerang-like shape of the loading and unloading curves at point E. The associated stiffness was 369 KN/cm/cm, which, when compared to the stiffness at point B (which was 482 KN/cm/cm), reflected a decrease of 23%. Thus, the reduction in stiffness could be a measure of the damage accumulated in the composite disk during the monotonic biaxial loading. This association, which also applies to cyclic flexing, was contrary to the composite response under uniaxial tensile loading. Because the failures were of a catastrophic nature, a decrease in stiffness due to composite damage did not occur in the latter case.[14]

The selection of 10% decrease in the maximum cyclic load under a constant cyclic strain range as the failure criterion was not arbitrary. The surface aluminum matrix underwent some strain hardening during cyclic flexing which, in combination with occasional surface cracks, could lead to a temporary 2.5% change in stiffness. In many cases, this 2.5% change in stiffness vanished with continuing cycling, probably due to a redistribution of the loads and the consequent matrix hardening. However, it was verified that once the stiffness decrease exceeded 5%, the decrease was permanent. A 10% decrease in stiffness was selected to achieve a safety factor of 2 that the decrease was permanent. Although continuing cyclic loading beyond this 10% decrease in stiffness did not lead to a catastrophic failure, the supported load had to be decreased by 10% in order to maintain a constant cyclic strain range.

With cyclic strain ranges greater than 0.004, the dominant damage mechanism leading to specimen failure was fiber fraction. Thus, the 25.4% decrease in load-carrying capacity shown in Figure 6 was solely due to fiber fractures. Experimental results suggested that a single valued relationship could exist between the cyclic strain range and the extent of the saturation damage introduced in the composite. The fiber crack density reached a saturation value of 2 to 3 cracks/mm in the first 0° ply after 16 cycles under a constant cyclic strain range of 0.00383. For cyclic strain ranges approaching the value of 0.003, the fiber crack density diminished, and defects in the matrix became more frequent. The latter defects were slip bands; cracks parallel to the plies and cracks forming a 30° angle with the disk's thickness (Figures 11, 12, and 14, respectively). A loss in stiffness could be attributed to the extent of the damage introduced in the composite during cyclic flexing. This finding was contrary to the cyclic uniaxial tensile loading of the composite where the failure was catastrophic and no loss in stiffness could be correlated to the damage.[14]

The limiting value of the maximum fiber cyclic strain under biaxial tension and for 10^{6} cycles of life was 0.00132. This limiting strain value was roughly 15% of the composite strain-to-failure under monotonic uniaxial tension. It was found in earlier work[14] that for a life span of 10^{6} cycles, the maximum cyclic fiber strain in uniaxial tensile fatigue was 0.00264. The latter limit is twice the magnitude of the strain range limit under cyclic biaxial tension. However, because the nature of the fatigue damage mechanisms under uniaxial tension was different from that under biaxial tension, these two cyclic strain limits were associated with composite failures which were quite different in nature. Under uniaxial conditions, the composite failure mechanism was random fiber fracture which led to a catastrophic specimen fracture. On the contrary, under biaxial loading, the failure related to a decrease in the load-carrying capacity which did not lead to a catastrophic failure on subsequent cycling.

SUMMARY AND CONCLUSIONS

The disk specimen was used to study the response of a continuous silicon carbon fiber-reinforced aluminum composite to biaxial tensile flexure. The maximum surface principal tensile strain was constant within a radius of 6.1 mm from the disk's center. This strain was found to be sensitive to the damage introduced in the composite during flexing. Fiber breakage under monotonic loading initiated within a fiber tensile strain 0.0038 to 0.0083. Under cyclic loading, and for principal surface strain ranges exceeding 0.0035, the dominant damage mechanism leading to failure was fiber breakage. At smaller surface strain ranges, slip bands and cracks formed in the matrix. The limiting value of the cyclic fiber strain range for a life of 10^6 cycles was 0.00132. This strain was 15% of the composite failure strain under uniaxial monotonic loading, and 50% of the maximum strain in uniaxial tensile fatigue.

REFERENCES

1. CHARVAT, M. H., and GARRETT, G. G. *The Development of a Closed Loop, Servo-Hydraulic Test System for Direct Stress Monotonic and Cyclic Crack Propagation under Biaxial Loading.* J. Testing and Evaluation, v. 8, no. 1, January 1980, p. 9-17.
2. PARSONS, M. W., and PASCOE, K. J. *Development of a Biaxial Fatigue Testing Rig.* J. Strain Analysis, v. 10, no. 1, 1975, p. 1-9.
3. PARSONS, M. W., and PASCOE, K. J. *Observations of Surface Deformation, Crack Initiation and Crack Growth in Low-Cycle Fatigue under Biaxial Stress.* Mat. Sci. and Engng., v. 22, 1976, p. 31-50.
4. PARSONS, M. W., and PASCOE, K. J. *Low-Cycle Fatigue under Biaxial Stress.* Proc. Instn. Mech. Engrs., v. 188, 61/74, 1974, p. 657-671.
5. LOHR, R. D., and ELLISON, E. G. *Biaxial High Strain Fatigue Testing of 1 Cr-Mo-V Steel.* Fatigue of Engng. Mat. and Struct., v. 3, 1980, p. 19-37.
6. BROWN, M. W., and MILLER, K. J. *Biaxial Cyclic Deformation Behavior of Steels.* Fatigue of Engng. Mat. and Struct., v. 1, 1979, p. 93-106.
7. BROWN, M. W., and MILLER, K. J. *High Temperature Low Cycle Biaxial Testing of Two Steels.* Fatigue of Engng. Mat. and Struct., v. 1, 1979, p. 217-229.
8. HUA, C. T., and SOCIE, D. F. *Fatigue Damage in 1045 Steel under Constant Amplitude Biaxial Loading.* Fatigue of Engng. Mat. and Struct., v. 7, no. 3, 1984, p. 165-179.
9. TANAKA, K., MATSUOKA, S., and KIMURA, M. *Fatigue Strength of 7075-T6 Aluminum Alloy under Combined Axial Loading and Torsion.* Fatigue of Engng. Mat. and Struct., v. 7, no. 3, 1984, p. 195-211.
10. SAUNDERS, I., and NUTTING, J. *Deformation of Metals to High Strains Using Combination of Torsion and Compression.* Metal Science, v. 18, December 1984, p. 571-575.
11. SOCIE, D. F., and SHIELD, T. W. *Mean Stress Effects in Biaxial Fatigue of Inconel 718.* J. of Engng. Mat. Technology, v. 106, July 1984, p. 227-232.
12. OLADIMEJI, M. K. *Plane-Stress Fraction Testing of Finite Sheets Under Biaxial Loads.* Exp. Mechanics, v. 23, no. 2, 1983, p. 217-227.
13. TSANGARAKIS, N. *The Notch-Fatigue Behavior of an Aluminum Composite Reinforced Unidirectionally with Silicon Carbide Fiber.* J. Compo. Mat., v. 21, no. 11, November 1987, p. 1008-1016.
14. TSANGARAKIS, N., ANDREWS, B. O., and CAVALLARO, C. *Mechanical Properties of Some Silicon Carbide Reinforced Aluminum Composites.* J. Compo. Mat., v. 21, no. 5, 1987, p. 481-492.
15. SWANSON, S. R., CHRISTOFOROU, A. P., and COLVIN G. E. Jr. *Biaxial Testing of Fibers Composites Using Tubular Specimens.* Exp. Mechanics, v. 28, no. 3, September 1988, p. 238-243.
16. KULAR, G. S., and THE, J. H. L. *The Bulging of Anisotropic Aluminum Sheets- A Comparison of Theory and Experiments.* Int. J. Mach. Tool Design, v. 12, no. 4, December 1972, p. 281-296.
17. JOVANE, F. *An Approximate Analysis of the Superplastic Forming of a Thin Circular Diaphragm: Theory and Experiments.* Int. J. of Mech. Sci., v. 10, no. 5, 1968, p. 403-427.
18. RANTA-ESKOLA, A. J. *Use of the Hydraulic Bulge Test in Biaxial Tensile Testing.* Int. J. Mech. Sci., v. 21, no. 8, 1979, p. 457-465.
19. RAGAB, A. R., and HABIB, O. E. *Determination of Equivalent Stress Versus Equivalent Strain Behavior of Superplastic Alloys in Biaxial Stress Systems.* Mat. Sci. and Engng., v. 64, no. 1, May 1984, p. 5-14.
20. WANG, N. M., and SHAMMAMY, M. M. *Comparison of Experimental and Theoretical Results for the Hydraustatic Bulging of Circular Sheets.* Exp. Mech., v. 11, no. 2, 1971, p. 71-75.
21. SHETTY, D. K., ROSENFIELD, A. R., DUCKWORTH, W. H., and HELD, P. R. *A Biaxial-Flexure Test for Evaluating Ceramic Strength.* J. American Ceramic Soc., v. 66, no. 1, January 1983, p. 36-42.
22. QUINN, G., and WIRTH, G. *Biaxial Static Fatigue of Silicon Nitride.* Proceedings of 3rd Int. Symposium on Ceramic Mat. and Comp. for Engines, Las Vegas, Nevada, November 1988.
23. NUNES, J. *Tensile Behavior of Silicon Carbide Filaments and Silicon Carbide Fiber Reinforced 6061 Aluminum.* Proceed. of the 39th Mech. Failure Prevention Group, Failure Mechan. in High Performance Materials, Cambridge Univ. Press, New York, NY, J. G. Early et al. ed., 1985.
24. MIL-HDBK-SD. Department of Defense, v. 1, June 1983.
25. TSANGARAKIS, N., GRUBER, J. J., and NUNES, J. *Non-Destructive Evaluation of Fatigue Damage in Alumina Fiber Reinforced Aluminum.* J. of Compo. Mat., v. 19, May 1985, p. 250-268.
26. JOHNSON, W. S. *Fatigue Damage Accumulation in Various Metal Matrix Composites.* NASA Techn. Mem. 89116, Langley Res. Center, Hampton, VA, March 1987.
27. JOHNSON, W. S., LUBOWINSKI, S. J., HIGHSMITH, A. L., BREWER, W. D., and HOOGSTRATEN, C. A. *Mechanical Characterization of SCS6/Ti-15-3 Metal Matrix Composites at Room Temperature.* NASA Techn. Mem. 1014, Wright-Patterson AFB, Ohio, April 1988.

DISTRIBUTION LIST

No. of Copies	To
1	Office of the Under Secretary of Defense for Research and Engineering, The Pentagon, Washington, DC 20301
	Commander, U.S. Army Laboratory Command, 2800 Powder Mill Road, Adelphi, MD 20783-1145
1	ATTN: AMSLC-IM-TL
	Commander, Defense Technical Information Center, Cameron Station, Building 5, 5010 Duke Street, Aiexandria, VA 22304-6145
2	ATTN: DTIC-FDAC
	Metals and Ceramics Information Center, Battelle Columbus Laboratories, 505 King Avenue, Columbus, OH 43201
1	ATTN: Mr. Robert J. Fiorentino, Program Manager
1	Defense Advanced Research Projects Agency, Defense Sciences Office/MSD, 1400 Wilson Boulevard, Arlington, VA 22209
	Headquarters, Department of the Army, Washington, DC 20314
1	ATTN: DAEN-RDM, Mr. J. J. Healy
	Commander, U.S. Air Force Wright Aeronautical Laboratories, Wright-Patterson Air Force Base, OH 45433
1	ATTN: AFWAL/MLC
1	AFWAL/MLLP, D. M. Forney, Jr.
1	AFWAL/MLBC, Mr. Stanley Schulman
1	AFWAL/MLLS, Dr. Terence M. F. Ronald
1	Edward J. Morrissey, AFWAL/MLTE, Wright-Patterson Air Force Base, OH 45433
	Commander, Army Research Office, P.O. Box 12211, Research Triangle Park, NC 27709-2211
1	ATTN: Information Processing Office
	Commander, U.S. Army Materiel Command, 5001 Eisenhower Avenue, Alexandria, VA 22333
1	ATTN: AMCLD
	Commander, U.S. Army Armament, Munitions and Chemical Command, Dover, NJ 07801
1	ATTN: Mr. Harry E. Pebly, Jr., PLASTEC, Director
	Commander, U.S. Army Aviation Systems Command, 4300 Goodfellow Blvd., St. Louis, MO 63120-1798
1	ATTN: AMSAV-GTD
1	AMSAV-E
1	AMCPEO-AV
	Director, U.S. Army Ballistic Research Laboratory, Aberdeen Proving Ground, MD 21005
1	ATTN: SLCBR-TSB-S (STINFO)
	Commander, U.S. Army Foreign Science and Technology Center, 220 7th Street, N.E., Charlottesville, VA 22901
1	ATTN: Military Tech
	Commander, U.S. Army Materiel Systems Analysis Activity, Aberdeen Proving Ground, MD 21005
1	ATTN: AMXSY-MP, H. Cohen
	Commander, U.S. Army Missile Command, Redstone Scientific Information Center, Redstone Arsenal, AL 35898-5241
1	ATTN: AMSMI-RD-CS-R/Doc
1	AMSMI-RLM

No. of Copies	To
	Commander, U.S. Army Belvoir Research, Development and Engineering Center, Fort Belvoir, VA 22060-5606
1	ATTN: STRBE-D
1	STRBE-FS, Fuel & Water Supply Division
1	STRBE-N
1	STRBE-VL
	Commander, U.S. Army Aviation Applied Technology Directorate, Aviation Research and Technology Activity (AVSCOM), Fort Eustis, VA 23604-5577
1	ATTN: SAVRT-TY-ATP, Mr. James Gomez, Aerospace Engineer
	Commander, U.S. Army Tank-Automotive Command, Warren, MI 48090
1	ATTN: AMSTA-RCKM
	Director, Benet Weapons Laboratory, LCWSL, USA AMCOM, Watervliet, NY 12189
1	ATTN: AMSMC-LCB-TL
1	AMSMC-LCB-PS, Dr. I. Ahmad
	David Taylor Naval Ship Research and Development Center, Annapolis, MD 21402
1	ATTN: Dr. Michael Vassilaros - Code 2814
	Office of Naval Technology, 800 N. Quincy Street, Arlington, VA 20017
1	ATTN: Mr. J. J. Kelly - Code MAT 0715
	Naval Research Laboratory, Washington, DC 20375
1	ATTN: Code 5830
1	Dr. G. R. Yoder - Code 6384
1	Dr. S. C. Sanday - Code 6370
	Chief of Naval Research, Arlington, VA 22217
1	ATTN: Code 471
1	Dr. Steven G. Fishman
	Naval Sea Systems Command, Washington, DC 20362
1	ATTN: Mr. Marlin Kinna - 62R4
	Naval Air Development Center, Warminster, PA 18974
1	ATTN: Dr. E. U. Lee - Code 60632
	Naval Surface Weapons Center, White Oak, Silver Spring, MD 20910
1	ATTN: John V. Foltz - Code R32
1	Dr. Herbert Newborn - Code R34
	National Aeronautics and Space Administration, Washington, DC 20546
1	ATTN: Mr. Michael A. Greenfield, Program Manager for Materials, Code RTM-6
	National Aeronautics and Space Administration, Lewis Research Center, Cleveland, OH 44135
1	ATTN: Dr. James A. DiCarlo, Mail Stop 106-1
	National Aeronautics and Space Administration, Marshall Space Flight Center, Huntsville, AL 35812
1	ATTN: R. J. Schwinghammer, EH01, Dir, M&P Lab
1	Mr. W. A. Wilson, EH41, Bldg. 4612
	The Boeing Vertol Company, P.O. Box 16858, Philadelphia, PA 19142
1	ATTN: Mr. Robert L. Pinckney, Mail Stop P62-06
1	Mr. Joseph W. Lenski, Jr., Mail Stop P32-09
	E. I. DuPont De Nemours and Company, Inc., Textile Fibers Department, Pioneering Research Laboratory, Experimental Station, Wilmington, DE 19898
1	ATTN: Blake R. Bichlmeir
1	Mr. Rex C. Claridge, TRW, Incorporated, Manufacturing Division, Mail Stop 01-2210, 1 Space Park, Redondo Beach, CA 90278
1	Dr. James A. Cornie, Materials Processing Center, Bldg. 3, Room 237, Massachusetts Institute of Technology, 77 Massachusetts Avenue, Cambridge, MA 01239

No. of Copies	To
1	Dr. Bhagwam K. Das, Engineering Technology Supervisor, The Boeing Company, P.O. Box 3999, Seattle, WA 98124
1	Leroy Davis, NETCO, 592 Dryad Road, Santa Monica, CA 9042-1318
1	Mr. Joseph F. Dolowy, Jr., President, DWA Composite Specialties, Inc., 21133 Superior Street, Chatsworth, CA 91311
1	Mr. Robert E. Fisher, President, AMERCOM, Inc., 8948 Fullbright Avenue, Chatsworth, CA 91311
1	Mr. Louis A. Gonzalez, Kaman Tempo, 816 State Street, Santa Barbara, CA 93101
1	Prof. James G. Goree, Dept. of Mechanical Engineering, Clemson University, Clemson, SC 29631
1	William F. Grant, AVCO Specialty Materials Division, 2 Industrial Avenue, Lowell, MA 01851
1	Mr. Jacob Gubbay, Charles Stark Draper Laboratories, 555 Technology Square, Mail Station 27, Cambridge, MA 02139
1	Dr. H. A. Katzman, The Aerospace Corporation, P.O. Box 92957 Los Angeles, CA 90009
	Lockheed California Company, Burbank, CA 91520
1	ATTN: Mr. Rod F. Simenz, Department of Materials and Processes
	Lockheed Georgia Company, 86 South Cobb Drive, Marietta, GA 30063
1	ATTN: Materials and Processes Engineering Department
1	Mr. James Carroll
	Materials Concepts, Inc., 666 Hague Avenue, Columbus, OH 43204
1	ATTN: Mr. Stan.J. Paprocki
1	Mr. David Goddard
1	Dr. Mohan S. Misra, Martin Marietta Aerospace, P.O. Box 179, Denver, CO 80201
1	Mr. Patrick J. Moore, Staff Engineer, Lockheed Missiles and Space Company, Organization 62-60, Building 104, P.O. Box 504, Sunnyvale, CA 94086
1	R. Byron Pipes, Professor & Director, Center for Composite Materials, University of Delaware, Newark, DE 19711
1	Dr. Karl M. Prewo, Principal Scientist, United Technologies Research Center, Mail Stop 24, East Hartford, CT 06108
1	Dr. B. W. Rosen, Materials Sciences Corporation, Gwynedd Plaza II, Bethlehem Pike, Spring House, PA 19477
1	Prof. Marc H. Richman, Division of Engineering, Brown University, Providence, RI 02912
1	Mr. Ronald P. Tye, Energy Materials Testing Laboratory, Biddeford Industrial Park, Biddeford, ME 04005
1	Prof. Franklin E. Wawner, Department of Materials Science, School of Engineering and Applied Sciences, University of Virginia, Charlotesville, VA 22903
1	Dr. Carl Zweben, General Electric Company, Valley Forge Space Center/M4018, P.O.Box 8555, Philadelphia, PA 19101
	Director, U.S. Army Materials Technology Laboratory, Watertown, MA 02172-0001
2	ATTN: SLCMT-TML
2	Authors

U.S. Army Materials Technology Laboratory
Watertown, Massachusetts 02172-0001
BIAXIAL FLEXING OF A FIBER-REINFORCED ALUMINUM COMPOSITE -
Nikos Tsangarakis and Marc S. Pepi

AD ______________
UNCLASSIFIED
UNLIMITED DISTRIBUTION

Technical Report MTL TR 89-70, July 1989, 17 pp-illus-table. D/A Project: 1L162105.AH42

Key Words

Fiber composites
Metal-matrix composites
Biaxial loading

Disks of silicon carbide continuous fiber-reinforced $[(0^\circ/90^\circ)_{4S}]$ aluminum were supported circumferentially on one side and loaded at the center of the other side with a pin. Maxima principal tensile surface strains were determined during flexing with strain gages. Failure under monotonic loading initiated on the convex side of the disks with the formation of multiple breaks in the first layer of fibers. With further flexing, cracking extended to inner fiber layers. Finally, fracture extended through the convex surface layer of the aluminum matrix. On cyclic flexing, fiber cracking was found to be the failure mechanism whenever the cyclic principal surface strain range was 0.0035 or greater. For cyclic strain ranges less than 0.0035, slip bands and cracks were formed in the matrix in addition to the cracks formed in the fibers. The cyclic strain range limit for 10^6 cycles of life was found to approach 0.0015. The latter limit corresponded to a maximum cyclic fiber strain of 0.00132, which is only 15% of the fiber strain to failure under monotonic uniaxial composite loading.

U.S. Army Materials Technology Laboratory
Watertown, Massachusetts 02172-0001
BIAXIAL FLEXING OF A FIBER-REINFORCED ALUMINUM COMPOSITE -
Nikos Tsangarakis and Marc S. Pepi

AD ______________
UNCLASSIFIED
UNLIMITED DISTRIBUTION

Technical Report MTL TR 89-70, July 1989, 17 pp-illus-table. D/A Project: 1L162105.AH42

Key Words

Fiber composites
Metal-matrix composites
Biaxial loading

Disks of silicon carbide continuous fiber-reinforced $[(0^\circ/90^\circ)_{4S}]$ aluminum were supported circumferentially on one side and loaded at the center of the other side with a pin. Maxima principal tensile surface strains were determined during flexing with strain gages. Failure under monotonic loading initiated on the convex side of the disks with the formation of multiple breaks in the first layer of fibers. With further flexing, cracking extended to inner fiber layers. Finally, fracture extended through the convex surface layer of the aluminum matrix. On cyclic flexing, fiber cracking was found to be the failure mechanism whenever the cyclic principal surface strain range was 0.0035 or greater. For cyclic strain ranges less than 0.0035, slip bands and cracks were formed in the matrix in addition to the cracks formed in the fibers. The cyclic strain range limit for 10^6 cycles of life was found to approach 0.0015. The latter limit corresponded to a maximum cyclic fiber strain of 0.00132, which is only 15% of the fiber strain to failure under monotonic uniaxial composite loading.

U.S. Army Materials Technology Laboratory
Watertown, Massachusetts 02172-0001
BIAXIAL FLEXING OF A FIBER-REINFORCED ALUMINUM COMPOSITE -
Nikos Tsangarakis and Marc S. Pepi

AD ______________
UNCLASSIFIED
UNLIMITED DISTRIBUTION

Technical Report MTL TR 89-70, July 1989, 17 pp-illus-table. D/A Project: 1L162105.AH42

Key Words

Fiber composites
Metal-matrix composites
Biaxial loading

Disks of silicon carbide continuous fiber-reinforced $[(0^\circ/90^\circ)_{4S}]$ aluminum were supported circumferentially on one side and loaded at the center of the other side with a pin. Maxima principal tensile surface strains were determined during flexing with strain gages. Failure under monotonic loading initiated on the convex side of the disks with the formation of multiple breaks in the first layer of fibers. With further flexing, cracking extended to inner fiber layers. Finally, fracture extended through the convex surface layer of the aluminum matrix. On cyclic flexing, fiber cracking was found to be the failure mechanism whenever the cyclic principal surface strain range was 0.0035 or greater. For cyclic strain ranges less than 0.0035, slip bands and cracks were formed in the matrix in addition to the cracks formed in the fibers. The cyclic strain range limit for 10^6 cycles of life was found to approach 0.0015. The latter limit corresponded to a maximum cyclic fiber strain of 0.00132, which is only 15% of the fiber strain to failure under monotonic uniaxial composite loading.

U.S. Army Materials Technology Laboratory
Watertown, Massachusetts 02172-0001
BIAXIAL FLEXING OF A FIBER-REINFORCED ALUMINUM COMPOSITE -
Nikos Tsangarakis and Marc S. Pepi

AD ______________
UNCLASSIFIED
UNLIMITED DISTRIBUTION

Technical Report MTL TR 89-70, July 1989, 17 pp-illus-table. D/A Project: 1L162105.AH42

Key Words

Fiber composites
Metal-matrix composites
Biaxial loading

Disks of silicon carbide continuous fiber-reinforced $[(0^\circ/90^\circ)_{4S}]$ aluminum were supported circumferentially on one side and loaded at the center of the other side with a pin. Maxima principal tensile surface strains were determined during flexing with strain gages. Failure under monotonic loading initiated on the convex side of the disks with the formation of multiple breaks in the first layer of fibers. With further flexing, cracking extended to inner fiber layers. Finally, fracture extended through the convex surface layer of the aluminum matrix. On cyclic flexing, fiber cracking was found to be the failure mechanism whenever the cyclic principal surface strain range was 0.0035 or greater. For cyclic strain ranges less than 0.0035, slip bands and cracks were formed in the matrix in addition to the cracks formed in the fibers. The cyclic strain range limit for 10^6 cycles of life was found to approach 0.0015. The latter limit corresponded to a maximum cyclic fiber strain of 0.00132, which is only 15% of the fiber strain to failure under monotonic uniaxial composite loading.